Polarization beam splitters, converters and analyzers based on a metasurface composed of regularly arranged silicon nanospheres with controllable coupling strength

Jin Xiang,[1] Jinxiang Li,[1] Hui Li,[1] Chengyun Zhang,[2] Qiaofeng Dai,[1] Shaolong Tie,[3] and Sheng Lan[1,*]

[1]*Guangdong Provincial Key Laboratory of Nanophotonic Functional Materials and Devices, School of Information and Optoelectronic Science and Engineering, South China Normal University, Guangzhou 510006, China*
[2]*School of Physics and Electronic Engineering, Guangzhou University, Guangzhou 510640, China*
[3]*School of Chemistry and Environment, South China Normal University, Guangzhou 510006, China*
[*]*slan@scnu.edu.cn*

Abstract: A metasurface composed of regularly arranged silicon (Si) nanospheres (NSs) with coupling was investigated both theoretically and numerically based on the Mie theory, the simple Lorentz line shape model and the finite-difference time-domain technique. By deliberately controlling the coupling strength between Si NSs through the design of the lattice constants of a rectangular lattice, polarization beam splitters, converters and analyzers with good performance can be successfully constructed. A square lattice as well as a large incidence angle was employed to build the polarization beam splitters and converters. At an incidence angle of 80°, the polarization beam splitters can completely reflect the *s*-polarized light and transmit the *p*-polarized light in a wavelength region of 510–620 nm. For a circularly polarized light incident on the polarization converters, one can get *s*-polarized light in the reflection direction and *p*-polarized light in the transmission direction. For the polarization beam analyzers, a rectangular lattice with deliberately chosen lattice constants was employed and the transmissivity of a linearly polarized light can be continuously adjusted from 0 to ~0.90 by simply rotating the metasurface. We revealed that the broadening of either the electric dipole resonance or the magnetic dipole resonance or both of them, which is induced by the asymmetric coupling of Si NSs, is responsible for the modification in the transmissivity spectrum of the metasurface. Our findings provide a guideline for designing photonic devices based on the metasurfaces composed of Si NSs with controllable coupling strength.

References and links

1. C. Enkrich, M. Wegener, S. Linden, S. Burger, L. Zschiedrich, F. Schmidt, J. F. Zhou, T. Koschny, and C. M. Soukoulis, "Magnetic metamaterials at telecommunication and visible frequencies," Phys. Rev. Lett. **95**(20), 203901 (2005).
2. N. Yu and F. Capasso, "Flat optics with designer metasurfaces," Nat. Mater. **13**(2), 139–150 (2014).
3. J. A. Schuller and M. L. Brongersma, "General properties of dielectric optical antennas," Opt. Express **17**(26), 24084–24095 (2009).
4. N. Fang, H. Lee, C. Sun, and X. Zhang, "Sub-diffraction-limited optical imaging with a silver superlens," Science **308**(5721), 534–537 (2005).

5. S. Sun, K. Y. Yang, C. M. Wang, T. K. Juan, W. T. Chen, C. Y. Liao, Q. He, S. Xiao, W. T. Kung, G. Y. Guo, L. Zhou, and D. P. Tsai, "High-efficiency broadband anomalous reflection by gradient meta-surfaces," Nano Lett. **12**(12), 6223–6229 (2012).

6. M. Decker, I. Staude, M. Falkner, J. Dominguez, D. N. Neshev, I. Brener, T. Pertsch, and Y. S. Kivshar, "High-efficiency dielectric Huygens' surfaces," Adv. Opt. Mater. **3**(6), 813–820 (2015).

7. B. Desiatov, N. Mazurski, Y. Fainman, and U. Levy, "Polarization selective beam shaping using nanoscale dielectric metasurfaces," Opt. Express **23**(17), 22611–22618 (2015).

8. S. Linden, C. Enkrich, M. Wegener, J. Zhou, T. Koschny, and C. M. Soukoulis, "Magnetic response of metamaterials at 100 terahertz," Science **306**(5700), 1351–1353 (2004).

9. Q. Zhao, J. Zhou, F. Zhang, and D. Lippens, "Mie resonance-based dielectric metamaterials," Mater. Today **12**(12), 60–69 (2009).

10. W. Liu, J. Zhang, B. Lei, H. Hu, and A. E. Miroshnichenko, "Invisible nanowires with interfering electric and toroidal dipoles," Opt. Lett. **40**(10), 2293–2296 (2015).

11. B. Dev Choudhury, P. K. Sahoo, R. Sanatinia, G. Andler, S. Anand, and M. Swillo, "Surface second harmonic generation from silicon pillar arrays with strong geometrical dependence," Opt. Lett. **40**(9), 2072–2075 (2015).

12. A. I. Kuznetsov, A. E. Miroshnichenko, Y. H. Fu, J. Zhang, and B. Luk'yanchuk, "Magnetic light," Sci. Rep. **2**, 492 (2012).

13. A. B. Evlyukhin, S. M. Novikov, U. Zywietz, R. L. Eriksen, C. Reinhardt, S. I. Bozhevolnyi, and B. N. Chichkov, "Demonstration of magnetic dipole resonances of dielectric nanospheres in the visible region," Nano Lett. **12**(7), 3749–3755 (2012).

14. Y. H. Fu, A. I. Kuznetsov, A. E. Miroshnichenko, Y. F. Yu, and B. Luk'yanchuk, "Directional visible light scattering by silicon nanoparticles," Nat. Commun. **4**, 1527 (2013).

15. J. M. Geffrin, B. García-Cámara, R. Gómez-Medina, P. Albella, L. S. Froufe-Pérez, C. Eyraud, A. Litman, R. Vaillon, F. González, M. Nieto-Vesperinas, J. J. Sáenz, and F. Moreno, "Magnetic and electric coherence in forward- and back-scattered electromagnetic waves by a single dielectric subwavelength sphere," Nat. Commun. **3**, 1171 (2012).

16. J. C. Ginn, I. Brener, D. W. Peters, J. R. Wendt, J. O. Stevens, P. F. Hines, L. I. Basilio, L. K. Warne, J. F. Ihlefeld, P. G. Clem, and M. B. Sinclair, "Realizing optical magnetism from dielectric metamaterials," Phys. Rev. Lett. **108**(9), 097402 (2012).

17. R. M. Bakker, D. Permyakov, Y. F. Yu, D. Markovich, R. Paniagua-Domínguez, L. Gonzaga, A. Samusev, Y. Kivshar, B. Luk'yanchuk, and A. I. Kuznetsov, "Magnetic and electric hotspots with silicon nanodimers," Nano Lett. **15**(3), 2137–2142 (2015).

18. J. Yan, P. Liu, Z. Lin, H. Wang, H. Chen, C. Wang, and G. Yang, "Directional Fano resonance in a silicon nanosphere dimer," ACS Nano **9**(3), 2968–2980 (2015).

19. J. A. Schuller, R. Zia, T. Taubner, and M. L. Brongersma, "Dielectric metamaterials based on electric and magnetic resonances of silicon carbide particles," Phys. Rev. Lett. **99**(10), 107401 (2007).

20. C. Enkrich, M. Wegener, S. Linden, S. Burger, L. Zschiedrich, F. Schmidt, J. F. Zhou, T. Koschny, and C. M. Soukoulis, "Magnetic metamaterials at telecommunication and visible frequencies," Phys. Rev. Lett. **95**(20), 203901 (2005).

21. J. Cheng, D. Ansari-Oghol-Beig, and H. Mosallaei, "Wave manipulation with designer dielectric metasurfaces," Opt. Lett. **39**(21), 6285–6288 (2014).

22. S. Liu, M. B. Sinclair, T. S. Mahony, Y. C. Jun, S. Campione, J. Ginn, D. A. Bender, J. R. Wendt, J. F. Ihlefeld, P. G. Clem, J. B. Wright, and I. Brener, "Optical magnetic mirrors without metals," Optica **1**(4), 250 (2014).

23. Z. H. Jiang, S. Yun, L. Lin, J. A. Bossard, D. H. Werner, and T. S. Mayer, "Tailoring dispersion for broadband low-loss optical metamaterials using deep-subwavelength Inclusions," Sci. Rep. **3**, 1571 (2013).

24. M. Farmahini-Farahani and H. Mosallaei, "Birefringent reflectarray metasurface for beam engineering in infrared," Opt. Lett. **38**(4), 462–464 (2013).

25. W. J. Padilla, A. J. Taylor, C. Highstrete, M. Lee, and R. D. Averitt, "Dynamical electric and magnetic metamaterial response at terahertz frequencies," Phys. Rev. Lett. **96**(10), 107401 (2006).

26. B. I. Popa and S. A. Cummer, "Compact dielectric particles as a building block for low-loss magnetic metamaterials," Phys. Rev. Lett. **100**(20), 207401 (2008).

27. C. Pfeiffer, N. K. Emani, A. M. Shaltout, A. Boltasseva, V. M. Shalaev, and A. Grbic, "Efficient light bending with isotropic metamaterial Huygens' surfaces," Nano Lett. **14**(5), 2491–2497 (2014).

28. U. Zywietz, A. B. Evlyukhin, C. Reinhardt, and B. N. Chichkov, "Laser printing of silicon nanoparticles with resonant optical electric and magnetic responses," Nat. Commun. **5**, 3402 (2014).

29. U. Zywietz, C. Reinhardt, A. B. Evlyukhin, T. Birr, and B. N. Chichkov, "Generation and patterning of Si nanoparticles by femtosecond laser pulses," Appl. Phys. A. **114**(1), 45–50 (2014).

30. A. B. Evlyukhin, C. Reinhardt, and B. N. Chichkov, "Multipole light scattering by nonspherical nanoparticles in the discrete dipole approximation," Phys. Rev. B **84**(23), 235429 (2011).

31. A. Ahmadi and H. Mosallaei, "Physical configuration and performance modeling of all-dielectric metamaterials," Phys. Rev. B **77**(4), 045104 (2008).

32. A. B. Evlyukhin, C. Reinhardt, A. Seidel, B. S. Luk'yanchuk, and B. N. Chichkov, "Optical response features of Si-nanoparticle arrays," Phys. Rev. B **82**(4), 045404 (2010).

33. B. Slovick, Z. G. Yu, M. Berding, and S. Krishnamurthy, "Perfect dielectric-metamaterial reflector," Phys. Rev. B **88**(16), 165116 (2013).

34. P. Moitra, B. A. Slovick, Z. Gang Yu, S. Krishnamurthy, and J. Valentine, "Experimental demonstration of a broadband all-dielectric metamaterial perfect reflector," Appl. Phys. Lett. **104**(17), 171102 (2014).
35. I. Staude, A. E. Miroshnichenko, M. Decker, N. T. Fofang, S. Liu, E. Gonzales, J. Dominguez, T. S. Luk, D. N. Neshev, I. Brener, and Y. Kivshar, "Tailoring directional scattering through magnetic and electric resonances in subwavelength silicon nanodisks," ACS Nano **7**(9), 7824–7832 (2013).
36. Y. Yang, W. Wang, P. Moitra, I. I. Kravchenko, D. P. Briggs, and J. Valentine, "Dielectric meta-reflectarray for broadband linear polarization conversion and optical vortex generation," Nano Lett. **14**(3), 1394–1399 (2014).
37. R. Paniagua-Domínguez, Y. F. Yu, A. E. Miroshnichenko, L. A. Krivitsky, Y. H. Fu, V. Valuckas, L. Gonzaga, Y. T. Toh, A. Y. Kay, B. Luk'yanchuk, and A. I. Kuznetsov, "Generalized Brewster effect in dielectric metasurfaces," Nat. Commun. **7**, 10362 (2016).
38. J. D. Joannopoulos, R. D. Meade, and J. N. Winn, *Photonic Crystals* (Princeton University Press, 1995).
39. P. Albella, M. A. Poyli, M. K. Schmidt, S. A. Maier, F. Moreno, J. J. Sáenz, and J. Aizpurua, "Low-loss electric and magnetic field-enhanced spectroscopy with subwavelength silicon dimers," J. Phys. Chem. C **117**(26), 13573–13584 (2013).
40. A. E. Miroshnichenko, A. B. Evlyukhin, Y. S. Kivshar, and B. N. Chichkov, "Substrate-induced resonant magnetoelectric effects for dielectric nanoparticles," ACS Photonics **2**(10), 1423–1428 (2015).
41. A. E. Miroshnichenko, B. Luk'yanchuk, S. A. Maier, and Y. S. Kivshar, "Optically induced interaction of magnetic moments in hybrid metamaterials," ACS Nano **6**(1), 837–842 (2012).

1. Introduction

Metamaterials are materials not found in nature but are composed of periodic arrangement of artificial magnetic and electric "atoms" that are smaller than the wavelength of light. These "atoms" are not real atoms but are artificial nanostructures comprised of many real atoms. It has been proposed and demonstrated that metamaterials with unique properties (e.g., negative refractive index) can be achieved by deliberately designing the permeability and permittivity of the constituent magnetic and electric atoms [1–3]. Typical magnetic and electric "atoms" include metallic split rings and wires. A metasurface composed of a single layer of such artificial atoms can be considered as a two-dimensional metamaterial. Although the thickness of the metasurface is smaller than the wavelength of light, it enables the realization of many interesting optical phenomena, such as perfect lenses, optical cloaking and negative refraction [4]. Typical examples for metasurfaces include reflect-arrays of metallic antennas that demonstrate the generalized law of reflection [5], highly-efficient transmission metasurfaces composed of Huygens' sources [6], and metasurfaces of dielectric nanostructures capable of performing polarization selective beam shaping [7] etc. So far, metamaterials working in the microwave and terahertz spectral regions have been successfully demonstrated and their device applications are fully explored. By reducing the dimension of the metallic split rings to several hundred nanometers, metamaterials with magnetic responses at 100 THz have been successfully demonstrated [8]. However, the construction of metamaterials operating in the visible and near infrared spectral regions remains to be a challenge because of the large loss of metals. To solve this problem, dielectric objects with large permittivity such as silicon (Si) [9–18], germanium (Ge) and tellurium (Te) [16] are considered as the most promising constituent elements for the metamaterials working in the optical frequency because of two reasons. First, such dielectric objects with large permittivity exhibit strong magnetic dipole resonances. Second, the loss of such dielectric objects is quite small as compared with their metallic counterparts. Since Si nanospheres (NSs) with diameters in the range of 100–200 nm exhibit strong magnetic dipole resonances in the visible to near infrared spectral region and much smaller ohmic loss relative to metallic split-ring resonators [19–27], they have been considered as the most promising candidate for the blocks of metamaterials in the optical frequency. Therefore, the fabrication and characterization of such Si NSs have received intensive and extensive studies in recent years [28,29].

So far, the physical properties of single Si NSs have been deeply investigated [30] and much attention has been paid to the interaction between them in dimers and regular arrays [17,18,30–35]. It has been shown that Fano resonances can be achieved in Si dimers by exploiting the interference between the broadened electric dipole resonance and the magnetic dipole resonance [18]. In particular, much effort has been devoted to the arrays composed of

regularly arranged Si NSs or nanocylinders, which can be used for the construction of functional devices [31–35]. In 2008, Ahmadi and Mosallaei presented the physical concept and performance analysis of all-dielectric metamaterials [31]. Then, Evlyukhin *et al.* analyzed theoretically the reflection and transmission properties of Si particle arrays by using the coupled-dipole equations and discussed the conditions for achieving low reflection and transmission of light in 2010 [32]. In 2013, Slovick *et al.* investigated theoretically a broadband all-dielectric metamaterial perfect reflector based on a single layer of regularly arranged Si NSs and more practically an array of Si microcubes on a SiO_2 substrate [33]. Very recently, Moitra *et al.* experimentally demonstrated such kind of perfect reflector, which exhibited nearly 100% reflection in the telecommunication band, by using a metasurface composed of Si nanocylinders [34]. In addition, Decker *et al.* investigated theoretically and demonstrated experimentally the realization of a metasurface that exhibits nearly 100% transmission over a broadband by using regularly arranged Si nanodisks [6]. In 2014, Yang *et al.* demonstrated broadband linear polarization conversion and optical vortex generation by using a dielectric meta-reflectarray. They suggested an alternative approach to plasmonic metasurfaces by replacing the metallic resonators in the conventional plasmonic metasurfaces with high-refractive-index silicon cut-wires in combination with a silver ground plane [36]. Very recently, Paniagua-Domínguez *et al.* reported the so-called generalized Brewster effect realized by using dielectric metasurfaces [37]. The main principle of such functional devices is to control the amplitude and phase of the device through the interaction between the incident light and the scattering elements. Since the scattering elements exhibit significant magnetic dipole resonances, the magnetic field component of the incident light needs to be taken into account when considering the interaction between the incident light and the scattering elements. Actually, a periodic arrangement of Si NSs is a photonic crystal (PC) which has been extensively studied in the last two decades and photonic bandgaps are expected to appear in the PC [38]. For a metasurface composed of a single layer of Si NSs, however, the concept of PC is not applicable because there is only one layer of Si NSs in the propagation direction of light. Instead, the constituent Si NSs in the metasurface are generally regarded as artificial atoms or Huygens' sources and the transmission or reflection spectrum of the metasurface can be modified by designing the electric and magnetic dipole resonances of single Si NSs [6,33–35]. Consequently, perfect transmission or reflection of light within a broadband can be realized by using a metasurface composed of only a single layer of Si NSs.

So far, the physical properties of all-dielectric metasurfaces have been analyzed based mainly on the calculation of their effective permittivity and permeability [33,34]. Actually, this method is quite successful for analyzing the metamaterials operating in the terahertz and infrared spectral regions with unit structures smaller than the wavelength of light [25–27]. For all-dielectric metasurfaces working in the visible and near infrared spectral regions, the dimensions of the constituent dielectric objects are comparable to the wavelength of light and a more precise method (e.g., the dipole coupling method) is needed [6]. Although Si NSs possess strong magnetic dipoles, their electric and magnetic dipole resonances are generally narrow in the absence of coupling. However, many applications of functional metamaterials arise from the strong coupling between the electric and magnetic dipole resonances, implying that the study of the effects of coupling on the electric and magnetic dipole resonances has a profound physical meaning [39-41]. In this article, we investigated the effects of coupling on the electric and magnetic dipole resonances of Si NSs and revealed the physical mechanism responsible for the modification in the transmission and reflection spectra of the metasurfaces based on the Mie theory, the simple Lorentz line shape model and the finite-difference time-domain (FDTD) technique. We demonstrated that the coupling strength between Si NSs can be controlled to realize polarization beam splitters, convertors and analyzers by deliberately designing the lattice constants of the metasurfaces.

2. Metasurface structure and theoretical and numerical methods

The metasurfaces studied in this work are composed of Si NSs regularly arranged on a rectangular lattice with lattice constants of d_1 and d_2 in the x and y directions, as schematically shown in Fig. 1. For practical applications, such arrays of Si NSs can be fabricated on a thin glass slide by using femtosecond laser ablation of a silicon-on-insulator wafer, as demonstrated Zywietz *et al.* in their previous works [28,29]. In addition, the constituent Si NSs can be replaced by Si nanocylinders or nanodisks which can be fabricated by using electron beam lithography and focused ion etching [6,34,35]. It has been confirmed by numerical simulation that the glass substrate has negligible influence on the electric and magnetic dipole resonances of Si NSs [40]. For simplicity, we consider only the metasurfaces without glass substrates in order to save the computational resource and the conclusions are also applicable for the metasurfaces with glass substrates. For simplicity, the diameter of Si NSs was fixed at $D = 170$ nm in this work and the lattice constants (d_1 and d_2) are the only two parameters used to characterize the metasurfaces and to control the coupling strength between Si NSs. The proposed devices operating in the visible to near infrared spectral region can be constructed with Si NSs with diameters ranging from 130 to 250 nm and with suitable lattice constants.

The scattering spectra of single Si NSs and Si dimers and the transmissivity spectra of Si metasurfaces were either calculated theoretically based on the Mie theory and simple Lorentz line shape model or simulated numerically by using the FDTD method. In the numerical simulations, we used a non-uniform grid with the smallest size of 2 nm. In addition, a perfectly matched layer boundary was employed for the calculation of the scattering spectra of Si dimers while a periodic boundary condition was employed for the calculation of the transmission spectra of Si metasurfaces.

In Fig. 1(a), we depict the principle of the proposed polarization beam splitter which is built with a metasurface composed of Si NSs arranged on a square lattice (i.e., $d_1 = d_2 = L$). In this case, the light is incident on the metasurface at a large incidence angle of θ which is defined as the angle between the incident light and the normal of the metasurface. Under this configuration, the *s*-polarized light is completely reflected while the *p*-polarized one gets nearly 100% transmitted. This function is quite similar to that of the well-known Wollaston prism which separates randomly polarized or unpolarized light into two orthogonal linearly polarized outgoing beams. If the incident light is circularly polarized, then the metasurface can serve as a polarization converter by which a linearly polarized light is obtained in both the transmission (*p*-polarized) and the reflection direction (*s*-polarized), as illustrated in Fig. 1(b). In this case, there is no requirement for the incidence angle which influence only the conversion efficiency. In Fig. 1(c), we show schematically the principle of the proposed polarization beam analyzer which is a metasurface in which Si NSs are arranged on a rectangular lattice. A linearly polarized light is incident normally on the metasurface and the angle between the polarization of the light and the x axis is defined as the polarization angle α. We will demonstrate later that the transmissivity of the linearly polarized light can be continuously adjusted from 0 to ~0.9 by simply rotating the metasurface, as schematically shown in Fig. 1(c).
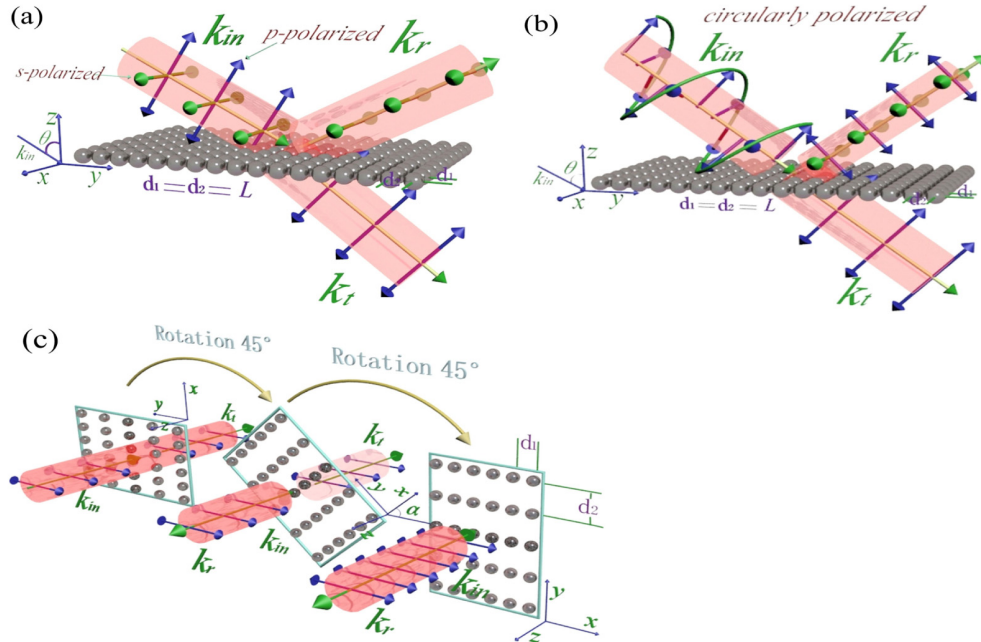
Fig. 1. Schematics showing (a) the polarization beam splitter ($d_1 = d_2 = L$, large θ), (b) the polarization beam converter ($d_1 = d_2 = L$, large θ), and (c) the polarization beam analyzer ($d_1 \neq d_2$, $\theta = 0°$) built with metasurfaces of Si NSs with different configurations. Here, the incidence angle is denoted as θ and the polarization angle is denoted as α. In each case, k_{in}, k_r, and k_t indicate the wavevectors for the incident, reflected, and transmitted light, respectively.

3. Results and discussion

3.1 Coupling-induced broadening in the electric and magnetic dipole resonances of a Si dimer: numerical simulation based on the FDTD method

In order to understand the coupling-induced modification in the electric and magnetic dipole resonances, let's first consider a Si dimer composed of two identical Si NSs with a diameter of $D = 170$ nm. The gap between the two Si NSs is denoted as g. Assuming light is incident on the Si dimer from the bottom, the polarization of the light can be either perpendicular or parallel to the axis of the Si dimer, as schematically shown in the insets of Fig. 2. When the magnetic field of the light is parallel to the axis of the dimer (or the light polarization is perpendicular to the axis of the dimer), a magnetic hotspot may be created in the gap if the distance between the two Si NSs is sufficiently small. Similarly, an electric hotspot will be generated in the gap provided that the separation between the two Si NSs is small enough. Such hot spots originate from the interaction between the electric or magnetic dipoles induced in the two Si NSs, implying the existence of coupling between them [17,39].

Now let's see what will happen to the linewidths of the electric and magnetic dipole resonances when the coupling strength between the two Si NSs is increased. We first calculated the scattering spectra of the two dimers with $g = 80$ and 0 nm under different illumination configurations based on the FDTD method. For the dimer with $g = 80$ nm, the coupling between the two Si NSs is negligible. In sharp contrast, a strong coupling between the two Si NSs is expected for the dimer with $g = 0$ nm. By fitting the scattering spectra with two symmetric Lorentz line shapes, we can easily derive the electric and magnetic dipole resonances for the dimer without coupling ($g = 80$ nm). For the dimer with strong coupling ($g = 0$ nm), we need to fit the scattering spectra with asymmetric line shapes in order to extract the electric and magnetic dipole resonances. The calculated scattering spectra and the

decomposed electric and magnetic dipole resonances for the two illumination configurations are presented in Figs. 2(a) and 2(b), respectively. In Fig. 2(a), it can be seen that the electric dipole resonance remains nearly unchanged when the gap in the dimer is reduced from 80 to 0 nm. Only a red shift of the magnetic dipole resonance is observed. Since the interaction between the two magnetic dipoles is dominant in this configuration, this behavior implies that the coupling between the magnetic dipoles has little influence on the linewidths of the electric and magnetic dipole resonances. In Fig. 2(b), a significant broadening of the electric dipole resonance is observed when the gap is reduced from 80 to 0 nm. In addition, a red shift as well as a broadening of the magnetic dipole resonance is found. This feature indicates that the coupling between the electric dipoles will induce a significant broadening in the linewidths of both the electric and the magnetic dipole resonances. In addition, the scattering cross sections for the two excitation schemes are different because they originate mainly from the coherent interaction between the electric and magnetic dipoles.
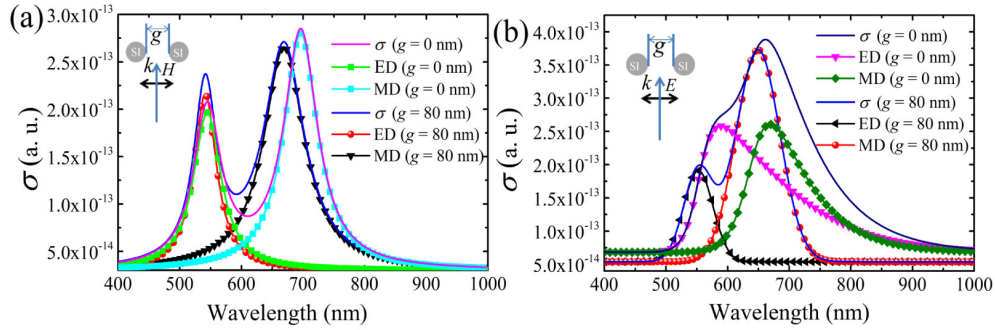

Fig. 2. Scattering spectra calculated for light polarization perpendicular (a) and parallel (b) to the axis of the dimers with g = 80 and 0 nm. The electric and magnetic dipole resonances were derived by fitting the scattering spectra by using symmetric Lorentz line shapes (a) and asymmetric Lorentz line shapes (b). Here, ED and MD represent the electric and magnetic dipole resonances, respectively.

In Fig. 2(b), it can be seen that the broadening of the electric dipole resonance observed in the Si NS dimer with g = 0 nm appears to be more significant that of the magnetic dipole resonance when the polarization of light is parallel to the axis of the dimer. It is because that the electric field of the electric dipole resonance extends more outside the Si NSs as compared with the electric field of the magnetic dipole resonance which exhibits a circular distribution inside the Si NSs. As a consequence, the overlap between the electric field of the two Si NSs is expected to be larger for the electric dipole resonance, leading to a stronger coupling strength and a more pronounced broadening. As demonstrated in the following, this unique feature for the coupling between Si NSs can be employed to construct photonic devices with different functionalities.

3.2 Coupling-induced broadening in the electric and magnetic dipole resonances: theoretical analysis based on the Mie theory

Based on the Mie theory, the scattering cross sections of a single Si NS can be decomposed into a series of multipolar contributions [18]:

$$\sigma_{scat} = \frac{2\pi}{k^2} \sum_{n=1}^{\infty} (2n+1)(|a_n|^2 + |b_n|^2). \tag{1}$$

Here, k is the wavevector of light, a_n and b_n demote the electric and magnetic Mie coefficients. For a metasurface composed of regularly arranged Si NSs, one can introduce effective dipole moments and polarizabilities to take into account the interaction or coupling

between the constituent Si NSs [6,32]. For light propagating along the z axis, the effective electric and magnetic polarizabilities of the metasurface can be expressed as follows:

$$\alpha_{eff}^{E} = \frac{1}{\dfrac{\varepsilon_0 \varepsilon_d}{\alpha^E} - k^2 \widehat{G}_{xx}^{0}}$$

$$\alpha_{eff}^{M} = \frac{1}{\dfrac{1}{\alpha^M} - k^2 \widehat{G}_{yy}^{0}} \qquad (2)$$

where $G0\ xx$ and $G0\ yy$ are the x and y components of the Green's tensor and α^E and α^M are the effective electric and magnetic polarizabilities of a single Si NS. Physically, α^E and α^M derived from the Mie coefficients for the electric and magnetic dipoles of a single Si NS [6,32] can be written as

$$\alpha^E = i\frac{6\pi\varepsilon_0\varepsilon_d}{k^3}a_1$$

$$\alpha^M = i\frac{6\pi}{k^3}b_1 \qquad (3)$$

In addition, the x and y components of the Green's tensor at far field approximation can be expressed as follows:

$$G_{xx}^{r} = G_{yy}^{r} \approx \frac{i}{2S_L k}e^{ik_d z} \qquad (4)$$

,

where S_L is the area of the lattice unit cell. It should be mentioned that the far-field approach is applicable for the metasurface with lattice constants smaller that the wavelength of light [6]. In this work, it was used to qualitatively discuss the effects of coupling on the linewidths of the effective electric and magnetic dipole resonances of a metasurface and the suitable lattice constants for realizing functional metasurfaces were obtained by using the FDTD simulation.

According to the Mie theory, we can easily calculate the scattering coefficients (a_1 and b_1) of a Si NS with D = 170 nm, as shown in Fig. 3(a). It can be seen that the electric and magnetic dipole resonances of a single Si NS possess narrow linewidths with negligible overlap. Based on Eqs. (3)-(5), we can derive the effective electric and magnetic polarizabilities of the metasurface, which represent the effective electric and effective magnetic dipole resonances, with different lattice constants ranging from 400 to 200 nm, as shown in Figs. 3(b) and 3(c). It can be seen that the electric and magnetic dipole resonances are broadened with decreasing lattice constant and the broadening of the electric dipole resonance appears to be more pronounced. This behavior is easily understood because for linearly-polarized light there are two types of coupling in Si metasurfaces, in contrast to the one type of coupling in Si dimers. For light polarized along the x axis, the coupling in the x direction is governed by the electric dipoles while that in the y direction is dominated by the magnetic dipoles. As compared with the electric dipoles, a smaller distance is needed in order to achieve an effective coupling between the magnetic dipoles.
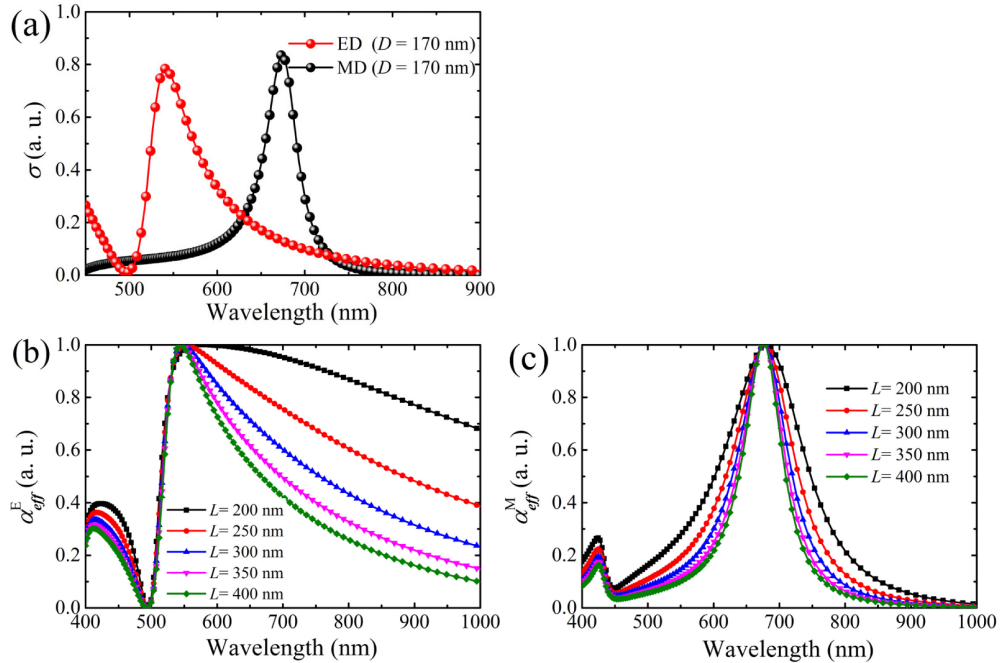
Fig. 3. (a) Effective electric and magnetic dipoles (a_1 and b_1) calculated for a single Si NS with $D = 170$ nm. The evolutions of the electric and magnetic polarizabilities of a metasurface composed of Si NSs arranged on a square lattice with decreasing lattice constant are shown in (b) and (c), respectively. Here, ED and MD represent the electric and magnetic dipole resonances, respectively.

3.3 Coupling-induced modification in the transmission spectra of the metasurface: numerical simulation based on the FDTD method

In order to gain a deep insight into the effects of coupling on the transmission properties of the metasurface, we simulated the transmissivity spectra of the metasurfaces (square lattice) with different lattice constants by using the FDTD method, as shown in Figs. 4(a) and 4(b). A periodic boundary condition was employed in the numerical calculation.
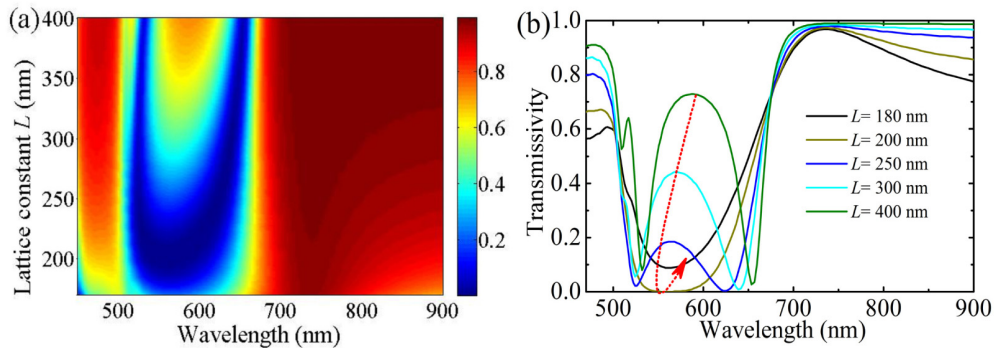

Fig. 4. (a) Dependence of the transmissivity on the wavelength of the incident light and the lattice constant calculated for the metasurface composed of Si NSs arranged on a square lattice calculated by using the FDTD simulation. (b) Evolution of the transmission spectrum of the metasurface with decreasing lattice constant.

It is noticed that a wavelength region (510–620 nm) with negligible transmissivity is obtained for the metasurface with L = 200 nm. Such a wavelength region is quite similar to a photonic bandgap commonly observed in PCs [38]. However, it is achieved by using only a single layer of Si NSs. For the metasurfaces with larger lattice constants, the transmissivity in the wavelength region increases because of the weakened coupling between Si NSs. In this case, a nearly 100% transmissivity is observed in the long-wavelength side of the magnetic dipole. For the metasurfaces with smaller lattice constants (e.g., L = 180 nm) in which a stronger coupling between Si NSs is expected, the transmissivity in this wavelength region also increases. This behavior indicates that a wavelength band with complete reflection can only be achieved in the metasurface in which the coupling strength between Si NSs has been deliberately controlled.

3.4 Underlying physical mechanism for the coupling-induced modification in the transmission spectra of metasurfaces

Physically, the transmission spectrum of a metasurface can be derived by considering the interference between the incident wave and the effective electric and magnetic dipoles of the metasurface. Assuming that the effective electric and magnetic dipoles possess equal strength, the complex transmission coefficient of the metasurface can be expressed as follows [6]:

$$t = 1 + \frac{2i\gamma_e\omega}{\omega_e^2 - \omega - 2i\gamma_e\omega} + \frac{2i\gamma_m\omega}{\omega_m^2 - \omega^2 - 2i\gamma_m\omega}. \qquad (5)$$

Here, the effective electric and magnetic dipoles, which correspond to the second and third terms in Eq. (5), are described as Lorentz line shapes with central frequencies of ω_e and ω_m and damping parameters of γ_e and γ_m. While the central frequencies ω_e and ω_m are mainly determined by the size of Si NSs, the damping parameters γ_e and γ_m are generally governed by the coupling between Si NSs. In practice, these parameters can be determined by experiments. In Fig. 5(a), we show the amplitude spectrum of the complex transmission coefficient calculated for a metasurface whose electric and magnetic dipoles possess equal strength and linewidth (γ_e and γ_m = 10π THz). The resonant frequencies of the electric and magnetic dipoles are chosen to be ω_e = 545 THz and ω_m = 447 THz, corresponding to the wavelengths of λ_e = 550 nm and λ_m = 670 nm. In this case, one can see two dips in the amplitude spectrum which originates from the destructive interference between the incident wave and the electric and magnetic dipoles. In the spectral region between the two dips, a large amplitude (or transmissivity) is observed. The phase spectrum for the complex transmissivity is shown in Fig. 5(b) where an abrupt change in the phase by π is observed at the electric and magnetic dipole resonances. Now we keep the resonant frequencies unchanged and increase the linewidths of the electric and magnetic dipoles to γ_e = 165π THz and γ_m = 75π THz, as shown in Fig. 5(c). In this case, a pronounced overlap between the electric and magnetic dipole resonances occurs. As a result, a transmissivity valley is formed in between the electric and magnetic dipole resonances, similar to the situation shown in Fig. 4. Since the linewidth of a dipole resonance characterizes the damping of the dipole, the broadening of the dipole resonance implies a faster decay of the dipole and it can be induced through the coupling of the constituent scatters of the metasurface. The phase spectrum for the metasurface with coupled scatters is shown in Fig. 5(d). It is noticed that a phase change of ~2π is observed across the transmissivity valley. However, there is almost no phase change in the spectral region of the transmissivity valley.
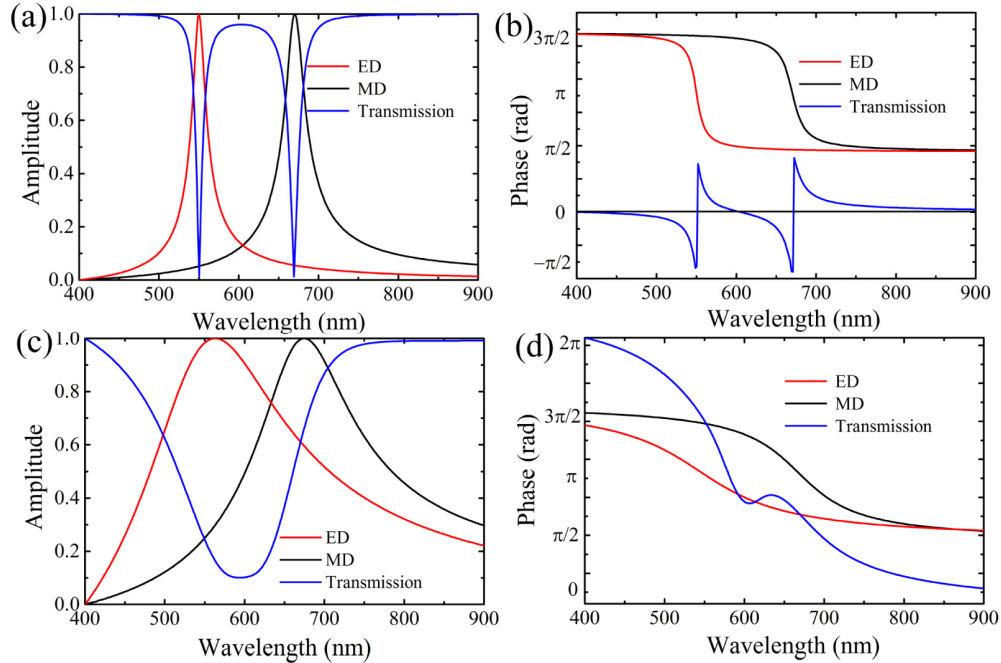
Fig. 5. Amplitude (a) and phase (b) spectra of the complex transmission coefficient calculated for the metasurface with equal electric and magnetic dipoles and narrow linewidths of $\gamma_e = 10\pi$ THz and $\gamma_m = 10\pi$ THz. The amplitude and phase spectra calculated for the metasurface with equal electric and magnetic dipoles and broadened linewidths of $\gamma_e = 165\pi$ THz and $\gamma_m = 75\pi$ THz are shown in (c) and (d). Here, ED and MD represent the electric and magnetic dipole resonances, respectively.

When we varied the lattice constant of the metasurface, the only parameter which is modified is the Green's tensor, as can be seen in Eq. (4). It is the variation of the Green's tensor that leads to the modification in the line shape of the effective electric and magnetic polarizabilities, as indicated in Eq. (2) and evidenced in Figs. 3(b) and 3(c). If we use the simplified model of Lorentz line shape to describe the effective polarizabilities and the transmissivity spectrum of the metasurface [see Eq. (5)], then the linewidths of electric and magnetic polarizabilities are mainly determined by the damping parameters γ_e and γ_m. The stronger the coupling between Si NSs, the larger the damping parameters are. As a result, a broadened line shape is expected for both the effective electric and magnetic polarizabilities. Therefore, the two methods used to describe the effective electric and magnetic polarizabilities of the metasurface reach the same conclusion of the linewidth broadening when the coupling between Si NSs is taken into account.

3.5 Polarization beam splitters and convertors based on the metasurfaces

In the case of normal incidence, one can expect the coupling between both the electric dipoles and the magnetic dipoles, leading to the simultaneous broadening of the linewidths of the electric and magnetic dipoles, as shown in Figs. 3(b) and 3(c). In this case, the transmissivity spectrum is almost independent of the polarization of the incident light. However, the situation is changed if we consider the case of oblique incidence and some interesting phenomena appear. By using the FDTD method, we simulated the transmission spectra of the metasurface composed of Si NSs arranged on a square lattice with a lattice constant of $L = 200$ nm for different incidence angles. The results for s- and p-polarized light are presented in Figs. 6(a) and 6(b), respectively. In Fig. 6(a), we can see that the wavelength region with negligible transmissivity remains nearly unchanged with increasing incidence angle. The only

change in the transmissivity spectrum is the reduction of the transmissivity on the long-wavelength side of the magnetic dipole. In comparison, it is noticed that the transmissivity in the wavelength region of 510−620 nm increases rapidly with increasing incidence angle and it reaches ~0.98 at an incidence angle of 80°.
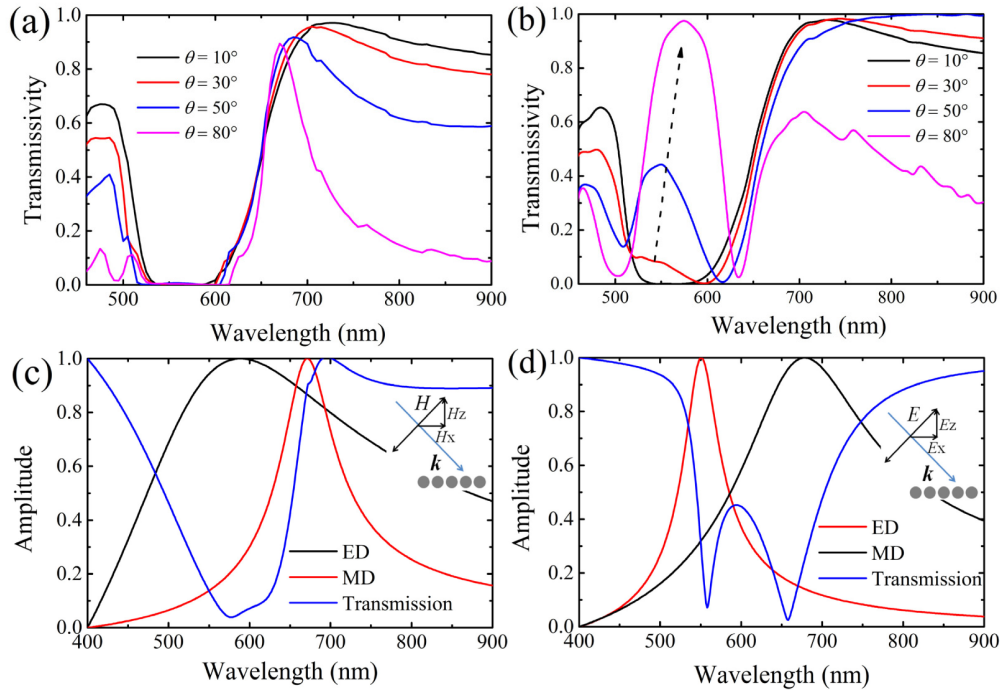

Fig. 6. Evolution of the transmission spectrum with increasing incidence angle for (a) *s*-polarized and (b) *p*-polarized light simulated for a metasurface composed of Si NSs arranged on a square lattice with a lattice constant of L = 200 nm. The amplitude (or transmissivity) spectrum for a metasurface composed of a broadened electric dipole (γ_m = 250π THz) and an un-broadened magnetic dipole (γ_m = 40π THz) is shown in (c) while that for a metasurface composed of an un-broadened electric dipole (γ_e = 40π THz) and a broadened magnetic dipole (γ_m = 250π THz) is shown in (d) by using the simplified Lorentz line shape model. Here, ED and MD represent the electric and magnetic dipole resonances, respectively.

The transmission properties shown in Fig. 6 can be interpreted by using the simple Lorentz line shape model described above. For the *s*-polarized light, the electric field (E_y) is parallel to the metasurface while the magnetic field can be decomposed into two components (H_x and H_z) that are parallel and perpendicular to the metasurface, as shown in the inset of Fig. 6(c). Only the component parallel to the metasurface (H_x) can induce coupled magnetic dipoles and lead to the broadening of the magnetic dipole resonance. With increasing incidence angle, the coupling between electric dipoles remains nearly unchanged while that between magnetic dipoles becomes weaker. As mentioned above, the influence of coupling strength on the linewidth of the magnetic dipole is not pronounced, as shown in Fig. 3(c). Therefore, the transmission spectrum is given by the interplay between a broadened electric dipole and an un-broadened magnetic dipole. As shown in Fig. 6(c), we calculated the amplitude (or transmissivity) spectrum of a metasurface with damping parameters of γ_e = 250π THz and γ_m = 40π THz, which correspond to a broadened electric dipole and an un-broadened magnetic dipole, and observed a wavelength region (550−650 nm) with very small transmissivity. The transmissivity in the wavelength region is not as small as that observed in the simulated transmissivity spectrum [see Fig. 6(a)] because of the simplicity of the Lorentz line shape model. Nevertheless, it interprets the underlying physical mechanism for the

formation of the reflection band. For the *p*-polarized light, the situation is reversed and one can expect the unchanged coupling between magnetic dipoles and the reduced coupling between electric dipoles with increasing incidence angle. As a result, the linewidth of the electric dipole is reduced at large incidence angles while that of the magnetic dipole is unchanged, as shown in Fig. 6(d). The calculated amplitude (or transmissivity) spectrum for the metasurface with two damping parameters of $\gamma_e = 40\pi$ THz and $\gamma_m = 250\pi$ THz, which correspond to an um-broadened electric dipole and a broadened magnetic dipole, exhibits an increase of transmissivity in the wavelength region of 550–650 nm with increasing incidence angle, in good agreement with the phenomenon observed in the simulated transmissivity spectrum shown in Fig. 6(b).

In practice, the strong dependence of the transmission spectrum on the polarization of the incident light at large incidence angles can be employed to build a polarization beam splitter which is schematically shown in Fig. 1(a). In Fig. 7(a), we present the dependence of the transmissivity on the incidence angle at a wavelength of 580 nm for the *s*- and *p*-polarized light. It can be seen that the transmissivity for the *s*-polarized light remains to be zero when the incidence angle is increased. In contrast, a rapid increase in the transmissivity with increasing incidence angle is observed for the *p*-polarized light. At an incidence angle of 80°, the transmissivity for the *p*-polarized light reaches 0.98. Therefore, an extremely good splitting between the *s*- and *p*-polarized light can be realized by using the metasurface at an incidence angle of 80°.
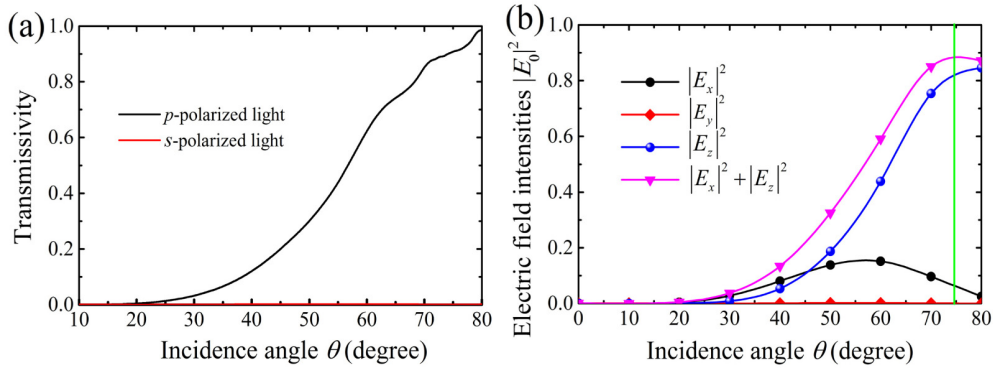

Fig. 7 (a) Dependence of the transmissivity of the *s*- and *p*-polarized light on the incidence angle at a wavelength of $\lambda = 580$ nm calculated for the metasurface composed of Si NSs arranged on a square lattice with a lattice constant of $L = 200$ nm. (b) Dependence of the electric field intensities ($|E_x|^2$, $|E_y|^2$, $|E_z|^2$, and $|E_x|^2 + |E_z|^2$) of the transmitted light on the incidence angle for the transmitted light.

For *s*-polarized light whose electric field is parallel to the metasurface, the transmissivity approaches zero for any incidence angle in the wavelength region of 510–620 nm. This feature can also be exploited to realize a polarization converter. As schematically shown in Fig. 1(b), a *p*-polarized light is achieved in the transmission direction when a circularly polarized light is incident on the metasurface. We calculated the dependence of the electric field intensities ($|E_x|^2$, $|E_y|^2$, $|E_z|^2$) of the transmitted light on the incidence angle for the metasurface, as shown in Fig. 7(b). It can be seen that for the transmitted light the *y* component of the electric field is completely removed for any incidence angle and only the *x* and *z* components are left. It means that the conversion of a circularly polarized light to a *p*-polarized one can be realized by using the metasurface. As shown in Fig. 7(b), the conversion efficiency is determined only by the incidence angle. While a monotonic increase is observed for $|E_z|^2$, a maximum value of of $|E_x|^2$ is found at ~60°. A calculation of the total electric field intensity ($|E_x|^2 + |E_z|^2$) as a function of the incidence angle indicates that the largest conversion efficiency is achieved at an incidence angle of ~74°. In this case, an extinction

ratio $[(|E_x|^2 + |E_z|^2)/|E_y|^2]$ as large as 5000 can be achieved for the *p*-polarized light. This value is much better as compared with that obtained by using the Brewster effect. In addition, there is no requirement for the incidence angle when using the metasurface as a polarization convertor and the incidence angle influences only the conversion efficiency.

3.6 Polarization beam analyzers based on the metasurfaces

So far, we have considered only metasurfaces in which Si NSs are arranged on a square lattice ($d_1 = d_2 = L$). In this case, the transmissivity of a linearly polarized light is almost independent of the polarization angle in the plane of the metasurface. If Si NSs are arranged on a rectangular lattice ($d_1 \neq d_2$), then a strong dependence of the transmissivity on the polarization angle is expected because the coupling strengths between Si NSs are much different along different directions. Since the coupling between electric dipoles is more sensitive to the distance between Si NSs, one can expect a strong coupling when the electric field is parallel to the short side of the rectangle and a weak coupling when the electric field is parallel to the long side of the rectangle. When the incident light is polarized along the short side of the rectangle, as shown in right part of Fig. 1(c), the electric dipoles are strongly coupled while the magnetic ones are weakly coupled. In this case, the incident light with wavelength in the overlapping zone of the electric and magnetic dipole resonances can be completely reflected due to the linewidth broadening of the effective electric dipole. When the incident light is polarized along the long side of the rectangle, as shown in the left part of Fig. 1(c), a large transmissivity is obtained because of the significantly reduced coupling between the electric dipoles. As shown in Fig. 4(b), the transmissivity in the wavelength region of 510−620 nm depends strongly on the distance between Si NSs and thus the coupling strength. Therefore, one can build a polarization beam analyzer by using a metasurface with a rectangular lattice.
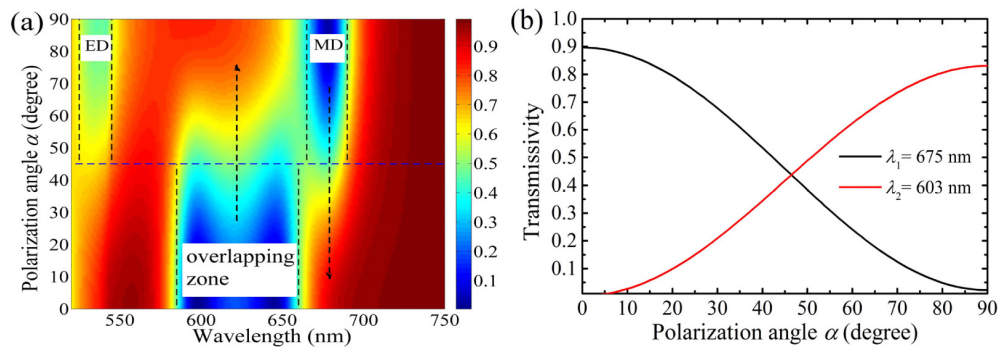

Fig. 8. (a) Dependence of the transmissivity on the wavelength and polarization of the incident light calculated for the metasurface composed of Si NSs arranged on a rectangular lattice with $d_1 = 280$ nm and $d_2 = 540$ nm. (b) Dependence of the transmissivity on the polarization angle of the incident light calculated for the metasurface at two different wavelengths of $\lambda_1 = 603$ nm and $\lambda_2 = 675$ nm.

In Fig. 8(a), we show the dependence of the transmissivity on the polarization angle and the wavelength of the incident light calculated for a metasurface with a rectangular lattice ($d_1 = 280$ nm, $d_2 = 540$ nm). It can be seen that there exists two wavelength regions in which the transmissivity can be adjusted by changing the polarization angle. One is located at the overlapping zone of the electric and magnetic dipoles (510−620 nm) and the other is located at the magnetic dipole resonance (665−685 nm). The evolution of the transmissivity with increasing polarization angle for two typical wavelengths is presented in Fig. 8(b). For $\lambda = 603$ nm, a monotonic increase in the transmissivity from 0 to ~0.84 is observed. In comparison, one finds a monotonic decrease in the transmissivity from ~0.90 to 0 for $\lambda = 675$

nm. Due to the large absorption of light at the wavelength of the electric dipole resonance, it cannot be used to realize a polarization analyzer because a significant change in the transmissivity with the polarization angle is not observed at this wavelength.

4. Conclusion

In summary, we have investigated analytically and numerically the transmission properties of metasurfaces composed Si NSs arranged on a rectangular lattice based on the Mie theory, the simple Lorentz line shape model and the FDTD technique. It was revealed that the transmission properties of such a metasurface are governed by the coupling between the electric and magnetic dipoles which leads to the linewidth broadening of the effective electric and magnetic dipoles of the metasurface. The coupling between the electric dipoles plays a dominant role in determining the transmission spectrum of the metasurface because it is more sensitive to the distance between Si NSs. By controlling the coupling strength between the constituent Si NSs through the design of the lattice constants of the metasurface, we have demonstrated the realization of polarization beam splitters which completely reflect *s*-polarized light and transmit *p*-polarized light. In addition, we can build polarization beam convertors which transform a circularly polarized light into a linearly polarized one. More interestingly, we have shown that highly efficient polarization beam analyzers can also be constructed by using metasurfaces with a rectangular lattice. All these behaviors indicate clearly that photonic devices with various functions can be constructed by exploiting the novel optical properties of metasurfaces composed of Si nanostructures (such as Si NSs, nanocylinders, and nanodisks etc.) with strong magnetic dipole resonance. Since the fabrication of such metasurfaces has been successfully demonstrated by using different techniques, we hope that the metasurface-based devices proposed in this work will be helpful for the design and fabrication of ultra-compact photonic functional devices.

Acknowledgments